
ERROR CORRECTION CODE TRANSFORMER: FROM NON-UNIFIED TO UNIFIED

Yongli Yan

Department of Electronic Engineering
Tsinghua University
yanyongli@tsinghua.edu.cn

Jieao Zhu, Tianyue Zheng, Jiaqi He

Department of Electronic Engineering
Tsinghua University
zja21, zhengty22, hejq24@mails.tsinghua.edu.cn

Linglong Dai

Department of Electronic Engineering
Tsinghua University
dail@tsinghua.edu.cn

ABSTRACT

Channel coding is vital for reliable data transmission in modern wireless systems, and its significance will increase with the emergence of sixth-generation (6G) networks, which will need to support various error correction codes. However, traditional decoders were typically designed as fixed hardware circuits tailored to specific decoding algorithms, leading to inefficiencies and limited flexibility. To address these challenges, this paper proposes a unified, code-agnostic Transformer-based decoding architecture capable of handling multiple linear block codes, including Polar, Low-Density Parity-Check (LDPC), and Bose-Chaudhuri-Hocquenghem (BCH), within a single framework. To achieve this, standardized units are employed to harmonize parameters across different code types, while the redesigned unified attention module compresses the structural information of various codewords. Additionally, a sparse mask, derived from the sparsity of the parity-check matrix, is introduced to enhance the model's ability to capture inherent constraints between information and parity-check bits, resulting in improved decoding accuracy and robustness. Extensive experimental results demonstrate that the proposed unified Transformer-based decoder not only outperforms existing methods but also provides a flexible, efficient, and high-performance solution for next-generation wireless communication systems.

1 Introduction

With the continuous evolution of wireless communication technologies, the imminent arrival of sixth-generation (6G) wireless communications heralds a paradigm shift towards ultra-reliable, low-latency communications and notably enhanced data rates [1, 2, 3]. To fulfill the ambitious performance requirements of 6G networks, probabilistic coding schemes are anticipated to play a crucial role. In particular, linear block codes such as Polar codes [4] and Low-Density Parity-Check (LDPC) codes [5] are expected to maintain their competitive edge established in fifth-generation (5G) wireless communications. These codes have also emerged as promising candidates for efficient error correction in 6G [6]. Additionally, another algebraic linear block code, known as the Bose-Chaudhuri-Hocquenghem (BCH) code [7], is often used as an outer code to enhance decoding performance.

1.1 Prior Works

Looking at 5G and earlier wireless communication systems, linear block code decoders were typically designed as fixed hardware circuits tailored to specific decoding algorithms. Looking ahead to 6G, this trend is likely to persist [8]. For instance, the Successive Cancellation (SC) decoding algorithm [4] for Polar codes uses a sequential method that traverses a decision tree to obtain the decoding result. This approach simplifies the hardware implementation of Polar codes by pruning binary trees [9]. In contrast, the Sum-Product (SP) decoding algorithm [10] for LDPC codes uses

iterative message passing, allowing for parallel data processing. This fundamentally differs from the sequential method used for Polar codes in hardware implementation [11]. Furthermore, BCH codes typically use algebraic decoding techniques [12], classified as hard decoding, which differs greatly from soft decoding methods like SC and SP. Overall, these algorithms provide strong error correction capabilities. However, due to the non-unified nature of the sequential and parallel architectures of Polar and LDPC codes, and the gap between hard and soft decoding in BCH codes, unique hardware circuits must be customized and fine-tuned for each specific linear block code. This may lead to significant engineering effort and inefficient use of hardware resources.

In an effort to reduce hardware resource consumption and establish a quasi-unified decoding framework, three methods have been explored: resource sharing, noise estimation, and Artificial Intelligence (AI)-driven approaches. Resource sharing involves time-sharing storage and computing units. Noise estimation methods decode various linear block codes by estimating the noise of received signals. Meanwhile, AI-driven methods offer a convenient way to unfold traditional algorithms like Belief Propagation (BP).

First, resource-sharing methods, such as those in [13] and [14], endeavor to integrate decoders for Polar and LDPC codes into a shared architecture based on traditional decoding algorithms. Both approaches aim to conserve hardware resources by temporally multiplexing the computational and storage units shared by the decoder through reconfiguration. However, due to the distinct decoding algorithms for each code type, achieving a truly unified architecture with such decoders is generally challenging.

Second, noise estimation methods were first proposed in [15] as the Guessing Random Additive Noise Decoding (GRAND) algorithm, used for Maximum Likelihood (ML) decoding of arbitrary codebooks in discrete channels, with or without memory [16, 17]. The algorithm operates by rank-ordering noise sequences based on their likelihood and subtracting them from the received signal to identify codebook members [16]. GRAND is shown to be capacity-achieving with random codebooks. However, this work faces the challenge of excessive guessing required by the GRAND algorithm, particularly for high logistic weights, which can lead to computational inefficiency. For instance, when the logistic weight equals 128, up to 5.33×10^7 queries may be necessary to complete a single decoding process [17].

Third, in recent years, AI-driven decoders have gained attention as an alternative. While model-based AI methods leverage traditional decoder algorithms and rely on neural networks to simulate belief propagation, their performance improvements are often limited by the constraints of conventional models [18], [19]. In contrast, model-free approaches offer a more flexible and scalable solution. Unlike model-based methods, which depend on predefined mathematical models, model-free approaches do not assume prior knowledge of the encoder or decoder. Instead, they rely on large amounts of labeled data to learn the decoding process directly, bypassing the limitations of conventional algorithms [20]. For example, inspired by the success of Transformers in Natural Language Processing (NLP) [21], a Transformer-based, model-free neural decoder called the Error Correction Code Transformer (ECCT) is proposed [22]. ECCT leverages the Transformer’s self-attention mechanism, where multiple attention heads work in parallel to effectively manage sequential data and capture long-range dependencies, to establish relationships between the input Log-Likelihood Ratios (LLRs) in the decoder. The inherent connection between Transformers and decoders lies in their shared ability to translate sequences—**whether from one language to another or from LLRs back to the original information bits**. However, despite offering greater flexibility, model-free approaches like ECCT still require frequent tuning of model parameters for each code type, length, and rate. This increases training costs and hardware overhead, making the decoding architecture non-unified.

1.2 Contributions

Thus, to reduce engineering efforts, training costs, and hardware consumption, we propose a unified, code-agnostic Transformer-based decoding architecture capable of handling multiple linear block codes, including Polar, LDPC, and BCH, within a single framework. To achieve this, we designed new standardized units and a unified attention module. Additionally, a sparse masking mechanism was developed to enhance decoding performance and stability¹. Specifically, the main contributions of this paper are summarized as follows.

1. **Unified Decoding Architecture:** We introduce a unified, code-agnostic Transformer decoding architecture, capable of seamlessly integrating various linear block codes. This architecture features standardized units to align various code lengths and, for the first time, designs a unified attention module that learns to compress the structural information of all codewords, thereby achieving a code-agnostic decoder. This architecture obviates the necessity for distinct hardware circuits for different decoding algorithms, reducing engineering efforts and hardware resource inefficiency.

¹Simulation codes will be provided to reproduce the results in this paper: <http://oa.ee.tsinghua.edu.cn/dailinglong/publications/publications.html>

2. **Standardized Units:** Standardized units are used to align parameters such as code length and code rate across different code types. Specifically, after receiving the channel output, we pad different codewords and their corresponding syndromes with zeros up to the maximum length. Through this unit, the Transformer neural decoder can accommodate any codeword within the maximum length, allowing for mixed training in a unified manner, thereby reducing training overhead.
3. **Unified Attention:** We redesigned the self-attention module to create a unified attention mechanism that allows different attention heads to share attention scores. This approach contrasts with traditional self-attention mechanisms, where each head independently computes its scores using separate learned weights. The unified attention compresses the structural information of different codewords through learning and shares parameters across various heads in the Transformer, resulting in a more cohesive decoding architecture. Additionally, we eliminated the need for iterations through the unified attention mechanism, thereby avoiding the detrimental effects of short cycles in Tanner graphs on LDPC belief propagation decoders. As a result, we have unlocked the full potential of LDPC codes, extending their applicability to short code scenarios.
4. **Performance Enhancement:** By introducing a sparse mask, which leverages the sparsity of the parity-check matrix, we have significantly enhanced the model’s ability to capture inherent constraints between information and parity-check bits. This has led to a substantial improvement in decoding performance and the achievement of a state-of-the-art design.
5. **High Computational Efficiency:** The unified attention module in our proposed Transformer-based decoding architecture demonstrates linear computational complexity by eliminating the need to project the input into higher dimensions. This results in a significant reduction in complexity from the traditional $O(N^2)$ to a more efficient $O(N)$, where N represents the sequence length. Additionally, by employing our sparse mask, we further achieve an 83% reduction in computational complexity. This efficiency gain enables faster processing and lower power consumption, making the architecture suitable for real-time applications in next-generation wireless communication systems.

The rest of this paper is organized as follows. Section II provides background knowledge, including the vanilla Transformers, channel encoders, as well as pre- and post-processing involved to address the issue of overfitting. Section III details our proposed unified code-agnostic Transformer. Section IV presents the results of training and inference. Section V analyzes the impact of the proposed optimization algorithms. Finally, Section VI concludes.

Notations: Lowercase and uppercase bold letters represent vectors and matrices, respectively. $\text{GF}(2)$ denotes the binary Galois field. \mathbb{R} represents real numbers. $[\cdot]^T$ stands for transpose, while $\mathcal{N}(\mu, \sigma^2)$ signifies a Gaussian distribution with mean μ and variance σ^2 . We define $\text{bipolar}(\cdot)$ to map binary to bipolar signals, and $\text{bin}(\cdot)$ represents its inverse mapping, where $\text{bipolar}(x)$ is defined as $1 - 2x$, and x takes values in the set $\{0, 1\}$. $\text{size}(\cdot)$ represents the number of elements in a matrix or vector. The sign function is denoted as $\text{sign}(\cdot)$.

2 Background

For a better understanding of the proposed unified error correction code Transformer, this section will provide background knowledge on vanilla Transformers and Forward Error Correction (FEC) codes.

2.1 Vanilla Transformers

The vanilla Transformer functions as a sequence-to-sequence model comprising an encoder and a decoder, both built from a series of L identical blocks. Each encoder block primarily integrates a multi-head self-attention module and a position-wise feed-forward network (FFN). To construct a deeper model and prevent gradient degradation, residual connections[23] are employed between the self-attention module and the FFN. Layer normalization[24] is applied to the inputs of each module, enhancing network stability and convergence speed. The overall architecture of the single-layer vanilla Transformer encoder is illustrated in Figure 1.

The following subsections will introduce the key modules within the vanilla Transformer.

2.1.1 Word Embedding

Word embedding is an important term in natural language processing, used to represent words for text analysis in the form of real-valued vectors. It enhances the computer’s ability to better understand text-based content. In this paper, word embeddings serve as reliability encoders that map the received one-dimensional signal to higher dimensions. It

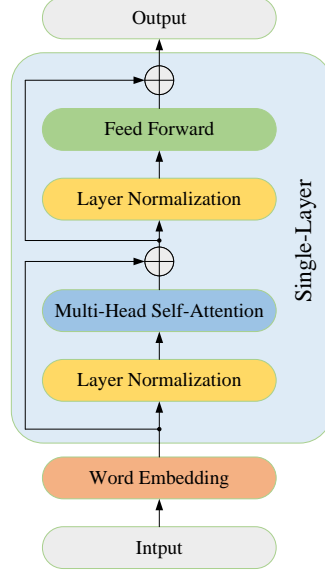


Figure 1: Overall architecture of the single-layer vanilla Transformer.

can be expressed as

$$Embedding(X) = X \odot \mathbf{E} \quad (1)$$

where $X \in \mathbb{R}^{N \times 1}$ is the received signal with length N and dimension one, $\mathbf{E} \in \mathbb{R}^{N \times d_k}$ represents the trainable embedding matrix with dimensions of d_k , and \odot denotes the Hadamard product.

2.1.2 Multi-Head Self-Attention

The vanilla Transformer establishes an attention mechanism based on the three Query-Key-Value (Q-K-V) matrices. It utilizes the \mathbf{Q} and \mathbf{K} matrices to establish correlations between different elements within the sequence and weights the \mathbf{V} matrix accordingly. The scaled dot-product form of attention is given by

$$Attention(\mathbf{Q}, \mathbf{K}, \mathbf{V}) = Softmax\left(\frac{\mathbf{Q}\mathbf{K}^T}{\sqrt{d_k}}\right) \mathbf{V} \quad (2)$$

$$Softmax(\mathbf{z})_i = \frac{e^{z_i}}{\sum_{j=1}^n e^{z_j}} \text{ for } i = 1, 2, \dots, n \quad (3)$$

where $\mathbf{Q} \in \mathbb{R}^{N \times d_k}$, $\mathbf{K} \in \mathbb{R}^{M \times d_k}$, $\mathbf{V} \in \mathbb{R}^{M \times d_v}$ represent tensors with lengths of N (for queries and keys) and M (for values), and dimensions of d_k (for queries and keys) and d_v (for values), respectively. The $Softmax(\cdot)$ function normalizes inputs into the range of 0 to 1, and to alleviate its gradient degradation issue, the dot product of queries and keys is divided by $\sqrt{d_k}$.

The study in[21] enhanced the attention layer by introducing a technique known as multi-head attention, which involves H different learned projection sets. This enhancement benefits the attention layer's performance in two significant ways: it widens the model's capacity to concentrate on various positions and grants the attention layer multiple representation subspaces. The multi-head attention can be written as

$$MultiHeadAttn(\mathbf{Q}, \mathbf{K}, \mathbf{V}) = Concat(head_1, head_2, \dots, head_H) \mathbf{W}^O \quad (4)$$

where $head_i = Attention(\mathbf{Q}\mathbf{W}_i^Q, \mathbf{K}\mathbf{W}_i^K, \mathbf{V}\mathbf{W}_i^V)$, and $\mathbf{W}_i^Q \in \mathbb{R}^{d_k \times d_k}$, $\mathbf{W}_i^K \in \mathbb{R}^{d_k \times d_k}$, $\mathbf{W}_i^V \in \mathbb{R}^{d_v \times d_v}$ are trainable parameters, $\mathbf{W}^O \in \mathbb{R}^{Hd_v \times Hd_v}$ is a weight matrix that was trained jointly with the model, serving to condense the outputs of different heads down into a single matrix.

If we set $\mathbf{Q} = \mathbf{K} = \mathbf{V} = \mathbf{X}$ in (4), the multi-head attention evolves into multi-head self-attention, where \mathbf{X} is the input of the neural network or the output from the previous layer. The architecture of multi-head self-attention is illustrated in Figure 2.

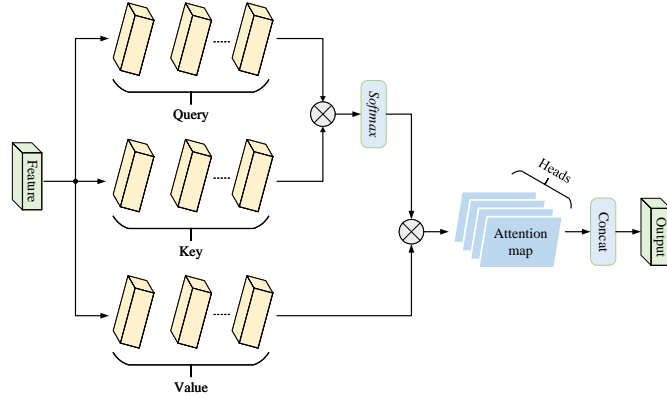


Figure 2: Architecture of multi-head self-attention.

2.1.3 Position-Wise Feed-Forward Network

The outputs of the self-attention layer are fed into the position-wise FFN layer. The position-wise FFN layer is essentially a fully connected network that operates uniformly on each position, and the non-linear activation function within it enables the Transformer to learn more complex feature representations. The mathematical expression for the FFN is as follows

$$FFN(\mathbf{X}) = \mathbf{W}_2 \times \text{ReLU}(\mathbf{W}_1 \times \mathbf{X} + \mathbf{b}_1) + \mathbf{b}_2 \quad (5)$$

$$\text{ReLU}(x) = \max(0, x) \quad (6)$$

where \mathbf{X} is the output of previous self-attention layer, and $\mathbf{W}_1 \in \mathbb{R}^{d_f \times d_h}$, $\mathbf{W}_2 \in \mathbb{R}^{d_h \times d_f}$, $\mathbf{b}_1 \in \mathbb{R}^{d_f}$, $\mathbf{b}_2 \in \mathbb{R}^{d_h}$ are trainable parameters, $d_h = H \times d_k$ is the dimensions of queries, keys and values, $\text{ReLU}(\cdot)$ represents the activation function. In general, to achieve better performance, d_f is set to be greater than d_h .

2.1.4 Residual Connection and Normalization

The multi-head self-attention layer and the position-wise FFN layer are connected through residual network[23] and layer normalization[24]. The overall architecture of each vanilla Transformer encoder can be written as

$$\begin{aligned} \mathbf{X}_1 &= \text{LayerNorm}(\text{MultiHeadAttn}(\mathbf{X}) + \mathbf{X}) \\ \mathbf{X}_2 &= \text{LayerNorm}(\text{FFN}(\mathbf{X}_1) + \mathbf{X}_1) \end{aligned} \quad (7)$$

where $\text{LayerNorm}(\cdot)$ denotes the layer normalization module.

2.2 Forward Error Correction Codes

In information theory, FEC is a technique designed to reduce the bit error rate (BER) when transmitting data over a noisy channel. We establish a standard linear block code utilizing a generator matrix \mathbf{G} with dimensions $k \times n$ and a parity-check matrix \mathbf{H} with dimensions $(n - k) \times n$. These matrices are specifically designed to satisfy $\mathbf{GH}^T = \mathbf{0}$ over the binary Galois field (GF).

We will now briefly discuss the encoder. The message vector $\mathbf{m} \in \{0, 1\}^k$ multiplied with the generator matrix \mathbf{G} over the GF(2) results in a codeword vector $\mathbf{x} \in \{0, 1\}^n$ satisfying $\mathbf{H}\mathbf{x} = \mathbf{0}$. The encoded codeword \mathbf{x} is modulated by Binary Phase Shift Keying (BPSK) to \mathbf{x}_s , where $\text{BPSK}(x) = 1 - 2x$. \mathbf{x}_s is transmitted through binary-input discrete memoryless channels (B-DMCs, e.g. an Additive White Gaussian Noise channel), resulting in a channel output $\mathbf{y} = \mathbf{x}_s + \mathbf{n}$, where \mathbf{n} is Gaussian noise with zero mean and variance σ^2 .

The goal of the decoder is to recover the transmitted message \mathbf{m} from the received signal \mathbf{y} . The overall architecture of the communication system including both encoding and decoding is illustrated in Figure 3. The objective of our work is to design and training of the parameterized decoding function f_θ .

To build a model-free Transformer decoding model, we draw inspiration from the pre- and post-processing methods proposed in [25], which have been demonstrated not to result in performance loss concerning bit error rate or mean

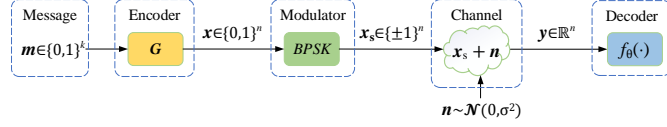


Figure 3: Architecture of the communication system.

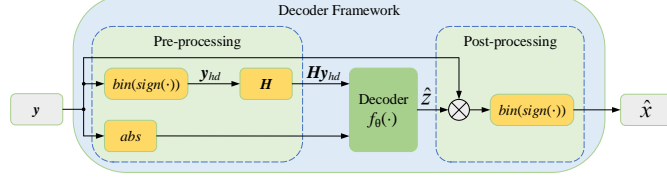


Figure 4: Decoder framework with pre- and post-processing.

squared error (MSE) metrics, as depicted in Figure 4. By training with an all-zero codeword to learn the noise, it is possible to avoid the overfitting problem that arises from the exponential growth of the codeword space with code length. And the B-DMCs is modeled by (8) which is an equivalent statistical mode that differs from the true physical one [26].

$$\mathbf{y} = \mathbf{x}_s \cdot \mathbf{z} \quad (8)$$

where \mathbf{z} is a random multiplicative noise independent of \mathbf{x}_s .

In the pre-processing step, the absolute values of received signal and the syndromes are concatenated as the input to the neural network, which can be written as

$$\tilde{\mathbf{y}} = [|\mathbf{y}|, s(\mathbf{y})] \quad (9)$$

where, $[\cdot, \cdot]$ denotes the concatenation of vectors, $|\mathbf{y}|$ signifies the absolute value of \mathbf{y} and $s(\mathbf{y}) \in \{0, 1\}^{n-k}$ represents the syndrome obtained by multiplying the parity check matrix with the hard decision of \mathbf{y} , defined as $s(\mathbf{y}) = \mathbf{H} \times \text{bin}(\text{sign}(\mathbf{y}))$.

In the post-processing step, the predicted multiplicative noise $\hat{\mathbf{z}}$ is multiplied by the received signal \mathbf{y} to recover \mathbf{x} . That is, the predicted $\hat{\mathbf{x}}$ takes the form

$$\hat{\mathbf{x}} = \text{bin}(\text{sign}(\mathbf{y} \cdot \hat{\mathbf{z}})) \quad (10)$$

3 Proposed Unified Error Correction Code Transformer

In this section, we present the complete architecture and training process of the proposed **Unified Error Correction Code Transformer (UECCT)**.

3.1 Unified Attention

The vanilla self-attention module can be viewed as establishing correlations among different input features within a data sample while neglecting the intrinsic relationships between different samples. This limitation hinders its ability to learn the distinctiveness of features between various code types in channel decoding tasks. Furthermore, research in [27] suggests that the output of the softmax function is probabilistically sparse, indicating that only a few weights dominate. This implies that an $N \times N$ self-attention matrix is not strictly necessary.

Based on the aforementioned considerations, we have developed a novel, low-complexity **Unified Attention Module (UAM)** to tackle channel decoding tasks involving multiple code types, lengths, and rates. We introduced learnable memory components, \mathbf{A}_l (attention) and \mathbf{V}_l (values), which play the role of learning features from the entire training dataset. The mathematical expression is given by

$$\text{UniAttn}(\mathbf{A}_l, \mathbf{V}_l) = \text{Softmax}(\mathbf{A}_l) \times \left(\mathbf{V}_l^T \mathbf{X} \right) \quad (11)$$

where $\mathbf{X} \in \mathbb{R}^{N \times d_k}$ is the input of attention layer, $\mathbf{A}_l, \mathbf{V}_l \in \mathbb{R}^{N \times d_l}$ are trainable parameters, and d_l is an adjustable hyperparameter.

Algorithm 1 Pseudocode for Multi-Head Unified-Attention

- 1 Input: \mathbf{X} # $shape = (B, N, d_h)$
 - 2 Trainable Parameters: $\mathbf{A}_l, \mathbf{V}_l$
 - 3 Hyper Parameters: H , number of heads; B , batch size
 - 4 Hyper Parameters: d_k , embedding size; $d_h = H \times d_k$
 - 5 $\mathbf{X} = \mathbf{X}.view(B, N, H, d_k).transpose(1, 2)$
 - 6 $\mathbf{V} = \mathbf{V}_l^T \times \mathbf{X}$ # $shape = (B, H, d_l, d_k)$
 - 7 $\mathbf{A} = \text{Softmax}(\mathbf{A}_l, dim = -1)$ # $shape = (B, 1, N, d_l)$
 - 8 $\mathbf{Out} = \mathbf{A} \times \mathbf{V}$ # $shape = (B, H, N, d_k)$
 - 9 $\mathbf{Out} = \mathbf{Out}.transpose(1, 2).view(B, N, d_h)$
 - 10 $\mathbf{Out} = \mathbf{W}^O(\mathbf{Out})$
 - 11 Output: \mathbf{Out} # $shape = (B, N, d_h)$
-

In order to gain a better understanding of the proposed UAM, we rewrite equation (2) as follows

$$\text{Attention}(\mathbf{W}^Q, \mathbf{W}^K, \mathbf{W}^V) = \text{Softmax}\left(\frac{(\mathbf{X}\mathbf{W}^Q) \times (\mathbf{X}\mathbf{W}^K)^T}{\sqrt{d_k}}\right) \times (\mathbf{X}\mathbf{W}^V) \quad (12)$$

where $\mathbf{W}^Q, \mathbf{W}^K, \mathbf{W}^V \in \mathbb{R}^{d_k \times d_k}$ are the projection matrices.

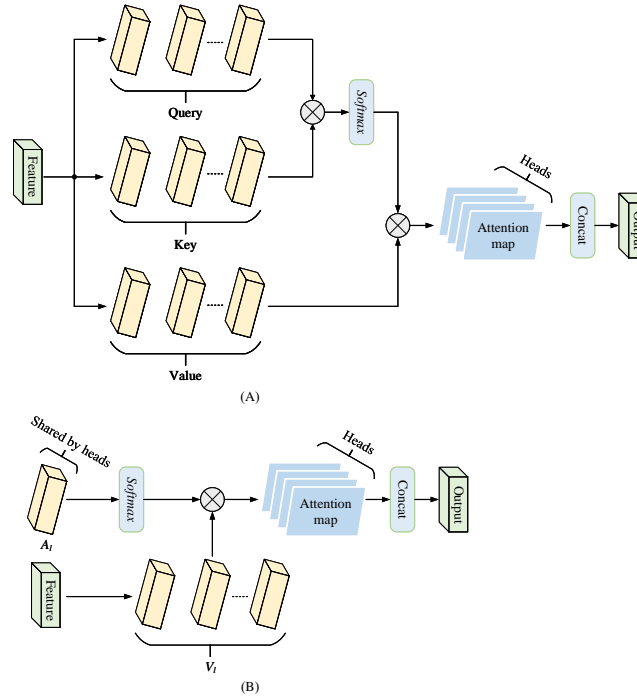


Figure 5: Architecture of the vanilla multi-head self-attention (A) and the proposed multi-head unified-attention (B).

Comparing equations (12) and (11), it is evident that the computational complexity of the vanilla self-attention module and the proposed UAM is $O(d_k \times N^2)$ and $O(d_k \times d_l \times N)$, respectively. Here, note that we omit the \mathbf{Q} and \mathbf{K} projections in the vanilla Transformer which results in further parameter savings. In fact, as observed in the subsequent experiments, a small value of d_l is sufficient to achieve a good bit error rate. Therefore, the proposed UAM is more suitable for large-scale inputs and is more accommodating to long channel codes compared to vanilla self-attention module. The proposed multi-head unified-attention and corresponding Python-style pseudocode are illustrated in Figure

5 and Algorithm 1, respectively. As depicted in Figure 5, thanks to the sparsity of the attention scores, multiple heads are able to share the same attention A_l , resulting in a more cohesive decoding architecture and further reducing the complexity of the neural network. This approach contrasts with vanilla self-attention mechanisms, in which each head independently computes its scores using separate learned weights.

3.2 Sparse Masked Attention

To detect and correct errors, a decoder needs to examine and contrast the received codeword using parity check equations, where a non-zero syndrome signals the presence of channel errors. In the Transformer architecture, attention is sparse as each parity bit does not correlate with every information bit. To address this, we propose enhancing the attention model with insights from human intelligence, which can clarify the dependencies between information and parity bits. By incorporating these dependencies, the model can more rapidly and accurately grasp the underlying principles of channel decoding, leading to enhanced performance.

Specifically, for any linear block code defined by a parity-check matrix $\mathbf{H} \in \mathbb{F}_2^{(n-k) \times n}$, we define a mapping function $M(\mathbf{H}) : \{0, 1\}^{(n-k) \times n} \rightarrow \{-\infty, 0\}^{N \times d_l}$. This function operates on \mathbf{H} and produces a mask that is applied to the attention memory A_l , such that

$$\text{UniAttn}(\mathbf{A}_l, \mathbf{V}_l) = \text{Softmax}(\mathbf{A}_l + M(\mathbf{H})) \times (\mathbf{V}_l^T \mathbf{X}) \quad (13)$$

Let A_l be a matrix in $\mathbb{R}^{N \times d_l}$, where N is defined as $2n - k$ and d_l as $n - k$. We naturally proceed to define the density of \mathbf{H} as

$$H_d = \frac{\text{sum}(\mathbf{H})}{(n - k) \times n} \quad (14)$$

We then construct the extended parity-check matrix $\bar{\mathbf{H}}$ as follows

$$\bar{\mathbf{H}} = \begin{bmatrix} \mathbf{H}^T \\ \mathbf{J}_{n-k} \end{bmatrix} \quad (15)$$

where \mathbf{J}_{n-k} is a randomly generated sparse matrix of size $(n - k) \times (n - k)$ with a density of H_d . The generation of the attention mask, therefore, becomes a direct process and is formulated as $M(\bar{\mathbf{H}})$.

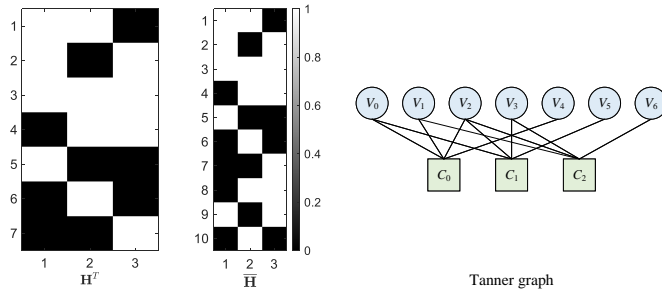


Figure 6: We present the corresponding matrices \mathbf{H}^T , $\bar{\mathbf{H}}$ and the Tanner graph for the Hamming (7,4) code.

For enhanced clarity, Figure 6 offers a visual depiction of matrices \mathbf{H}^T , $\bar{\mathbf{H}}$ and the Tanner graph, utilizing the Hamming (7,4) code as an illustrative example. Here, matrix \mathbf{H} is defined as

$$\mathbf{H} = \begin{bmatrix} 1 & 1 & 1 & 0 & 1 & 0 & 0 \\ 1 & 0 & 1 & 1 & 0 & 1 & 0 \\ 0 & 1 & 1 & 1 & 0 & 0 & 1 \end{bmatrix} \quad (16)$$

This illustration demonstrates that the application of the mask results in sparser attention, a phenomenon particularly pronounced in low-density parity-check codes. Most importantly, the complexity of the UAM is now reduced to the density of the code $O(H_d \times d_k \times d_l \times N)$. Our experimental results indicate that the use of this mask has successfully reduced the computational complexity of the attention mechanism by an average of 83%. Furthermore, we provide a summary of the Python-style sparse mask construction within Algorithm 2.

Algorithm 2 Pseudocode for Sparse Mask Construction

- 1 Input: \mathbf{H} # *shape* = $(n - k, n)$
 - 2 $H_d = \frac{\text{sum}(\mathbf{H})}{(n-k) \times n}$
 - 3 $\bar{\mathbf{H}} = \text{zeros}(2n - k, n - k)$
 - 4 $\bar{\mathbf{H}}[0 : n, 0 : n - k] = \mathbf{H}.\text{transpose}(0, 1)$
 - 5 $\bar{\mathbf{H}}[n : 2n - k, 0 : n - k] = \text{rand}(n - k, n - k) < H_d$
 - 6 Output: $(-\infty) \cdot (-\bar{\mathbf{H}})$
-

3.3 Architecture and Training

The architecture of the proposed unified error correction code Transformer is illustrated in Figure 7. The primary innovation in our model involves substituting the vanilla attention mechanism with a multi-head unified-attention module. This modification not only decreases computational complexity but also empowers the model to discern distinctive features among diverse codewords, thereby facilitating the establishment of a unified decoding architecture. We incorporate advanced pre-training strategies to optimize the model’s error correction performance. Furthermore, we have designed standardization units to standardize the lengths of codewords and syndromes across diverse datasets, ensuring the model’s compatibility with various code types, lengths, and rates.

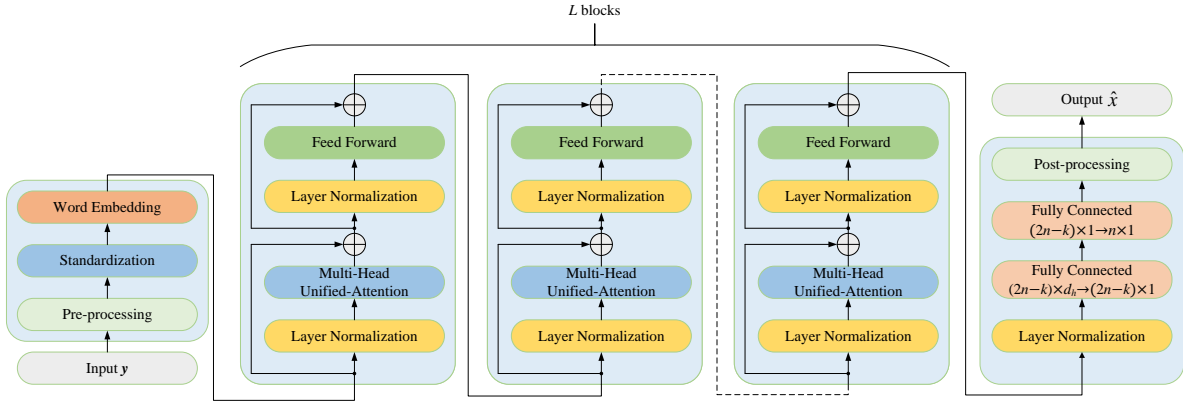


Figure 7: Illustration of the proposed unified error correction code Transformer.

In Figure 7, the output \mathbf{y} from the AWGN channel passes through the pre-processing module to yield $N = 2n - k$ input elements for the neural network. The decoder is constructed by concatenating L Transformer encoders, which consist of unified-attention and feed-forward layers, with normalization layers in between. The output module is characterized by two fully connected layers. The initial layer compresses the multi-head output into a one-dimensional vector of size $2n - k$, with the subsequent layer transforming it into an n -dimensional vector representing the softly decoded noise. Finally, the post-processing module acts on the estimated noise to derive the transmitted original codeword.

We employ binary cross-entropy as the loss function with the objective of learning to predict the multiplicative noise \mathbf{z} . The corresponding target binary multiplicative noise is denoted as $\tilde{\mathbf{z}} = \text{bin}(\text{sign}(\mathbf{z}))$. Therefore, the loss calculation for a received individual codeword \mathbf{y} is given by

$$\text{loss} = - \sum_{i=1}^n \tilde{z}_i \log(f_\theta(y)) + (1 - \tilde{z}_i) \log(1 - f_\theta(y)) \quad (17)$$

To accommodate codewords of varying lengths within a unified architecture, we have designed a standardization unit that performs padding on $|\mathbf{y}|$ and $s(\mathbf{y})$ as described in Equation (9). Specifically, after receiving the channel output, we pad different codewords and their corresponding syndromes with zeros up to the maximum length. Assuming that the maximum length of the codeword is N_{max} and the maximum length of the syndrome is S_{max} , the dataset is standardized according to

$$\tilde{\mathbf{y}} = [[|\mathbf{y}|, \mathbf{0}_c], [s(\mathbf{y}), \mathbf{0}_s]] \quad (18)$$

where $\mathbf{0}_c$ and $\mathbf{0}_s$ represent zero vectors with sizes $N_{max} - size(\mathbf{y})$ and $S_{max} - size(s(\mathbf{y}))$, respectively. Through this unit, the Transformer neural decoder can accommodate any codeword within the maximum length, allowing for mixed training in a unified manner.

In the training phase, we conducted 1000 epochs, each consisting of 1024 minibatches, which in turn contained 512 samples each. Samples for each minibatch were randomly selected from a pool of systematic Polar[28], LDPC, and BCH codewords. The learning rate was initialized at 10^{-3} , and a cosine decay scheduler was applied without warmup [29], gradually reducing it to 10^{-6} by the end of the training process. We employ the Adam optimizer to dynamically adjust the learning rate, leveraging its efficacy in managing diverse data types and model architectures [30]. The AWGN noise introduced to the links had its signal-to-noise ratio (SNR) randomly chosen between 4 and 6 for each batch. In the pre-training phase, we conducted 1000 epochs while maintaining consistency with all other parameters from the training phase. The word embeddings acquired during the pre-training stage served as the initial values for the subsequent training phase. The training and experiments were performed on NVIDIA GeForce RTX 4090 24GB GPUs.

4 Experiments

We conducted experiments on linear block codes, specifically Polar, LDPC, and BCH, to assess the effectiveness of the proposed architecture. The parity-check matrices utilized in the paper were sourced from [31]. We benchmark our approach against the most recent state-of-the-art performance reported in [22], where each codeword parameter was trained individually and also contrast it with the legacy successive cancellation list decoding algorithm for Polar codes [32], as well as the normalized min-sum decoding algorithm for LDPC codes [10] [33]. The results are presented in the form of bit error rate (BER) and block error rate (BLER) at various normalized SNR (i.e. E_b/N_0) values, with at least 10^6 random codewords tested for each. The terms CBER and CBLER are hereby defined to denote the comprehensive bit error rate and block error rate, respectively, for the entirety of codewords utilized, spanning Polar, LDPC, and BCH codes.

The proposed unified error correction code Transformer is defined by the following hyperparameters: the number of Transformer encoder layers L , the dimensions of word embeddings d_k , and the dimensions d_l of the trainable memory A_l and V_l along with the number of unified attention heads H . We present the performance of our framework for four different architectures with $L \in \{3, 6\}$, $d_k \in \{16, 32\}$, while all other hyperparameters are set to their default values: $d_l = 64, H = 8$. The hyperparameters in [22] are set as follows: $L = 6, d_k = 32, H = 8$. Additionally, for Polar SCL decoding, the list size is set to 8, and for LDPC NMS decoding, the maximum number of iterations is set to 15 with a normalized factor of 0.875.

Table 1 presents the simulation results, specifically showing the negative logarithm base 10 of the BER at E_b/N_0 values of 4, 5, and 6 dB. It is noted that higher values in this context are indicative of better performance. The best performance for each SNR is highlighted in bold and italics. We provide additional BER plots for Polar and LDPC codes in Figure 8 and Figure 9, respectively. Experimental results indicate that our approach achieves comparable performance to models trained individually as reported in [22], and outperforms both the SCL algorithm for Polar codes and the NMS algorithm for LDPC codes. Our proposed unified code-agnostic Transformer effectively decodes a wide range of code types, lengths, and rates. Especially for short LDPC codes, traditional NMS algorithms are constrained by a smaller girth, leading to poor performance because LLR information cannot propagate effectively during the iteration process. In contrast, our approach sidesteps this issue by eliminating iteration, thereby offering a practical solution for short LDPC code applications, such as those for future 6G mobile communication control channel coding schemes. Furthermore, the performance gains observed with smaller dimensions $d_l = 64 \ll N = 192$ confirm that the proposed decoding architecture substantially reduces computational complexity.

5 Analysis

We delve into the influence of Transformer encoder layers on overall performance, examining both the role of the dimension parameter d_k and the efficacy of sparse masked attention mechanisms. Furthermore, we conduct a comparative analysis of the computational complexity inherent in our methodology versus that of alternative approaches.

5.1 Impact of the Transformer Encoder Layers and the Dimensions d_k

Figure 10 illustrates the CBER performance across various Transformer encoder layers and the dimensions d_k . It can be observed that the number of Transformer encoder layers exerts a greater impact on performance than the dimension d_k . This increase in depth effectively enlarges the parameter search space, potentially enhancing the model’s nonlinear fitting capability and enabling more complex expression.

Table 1: A comparison of the negative logarithm base 10 of the BER

Method	SCL/NMS			ECCT			Ours			Ours			Ours					
	$L = 6, d_k = 32$	$L = 6, d_k = 32$	$L = 6, d_k = 32$	$L = 3, d_k = 16$	$L = 3, d_k = 16$	$L = 3, d_k = 16$	$L = 3, d_k = 32$	$L = 3, d_k = 32$	$L = 3, d_k = 32$	$L = 6, d_k = 16$	$L = 6, d_k = 16$	$L = 6, d_k = 16$	$L = 6, d_k = 32$	$L = 6, d_k = 32$	$L = 6, d_k = 32$			
E_b/N_0 [dB]	4	5	6	4	5	6	4	5	6	4	5	6	4	5	6			
Polar (32, 16)	2.71	3.43	4.22	2.68	3.45	4.38	2.41	3.15	4.03	2.50	3.25	4.05	2.65	3.43	4.33	2.79	3.60	4.52
Polar (64, 42)	2.86	3.75	4.63	2.72	3.72	4.89	2.41	3.27	4.38	2.49	3.42	4.59	2.70	3.71	4.91	2.87	3.91	5.22
Polar (128, 96)	2.74	3.68	4.76	2.86	4.03	5.30	2.25	3.14	4.41	2.33	3.31	4.63	2.52	3.65	5.07	2.71	3.92	5.47
LDPC (32, 24)	2.03	2.54	3.08	2.44	3.10	3.83	2.30	2.96	3.72	2.37	3.03	3.81	2.42	3.09	3.86	2.45	3.11	3.85
LDPC (64, 42)	2.87	3.89	4.94	3.01	4.17	5.42	2.47	3.31	4.45	2.55	3.51	4.64	2.90	4.03	5.49	3.00	4.20	5.87
LDPC (128, 64)	3.44	4.26	5.16	3.57	4.44	5.39	2.77	3.69	4.81	2.91	3.88	5.02	3.36	4.27	5.28	3.54	4.46	5.55
BCH (63, 36)	-	-	-	2.09	2.93	4.15	1.73	2.30	3.16	1.80	2.43	3.35	1.92	2.67	3.77	2.00	2.82	4.00

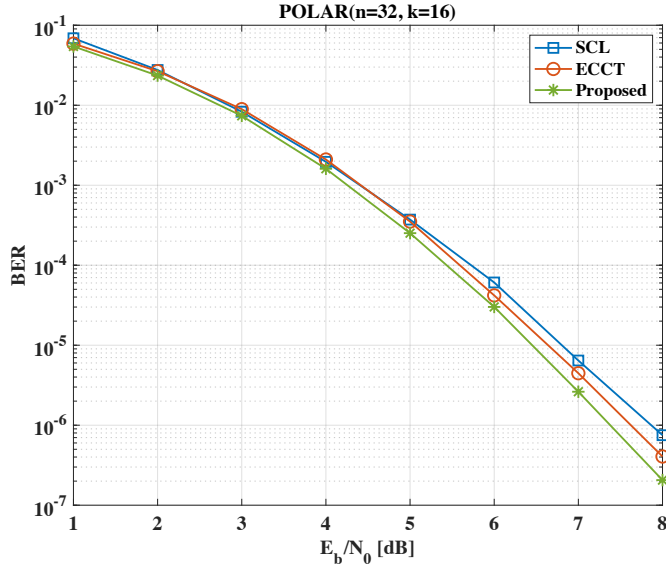


Figure 8: BER for Polar codes under $L = 6, d_k = 32$.

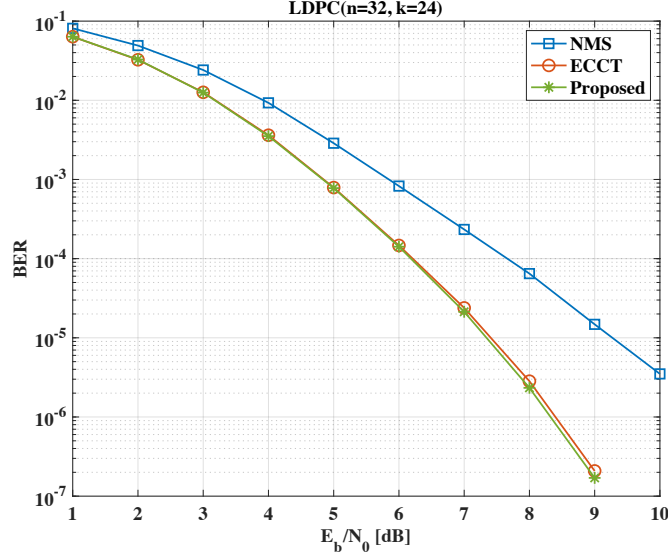
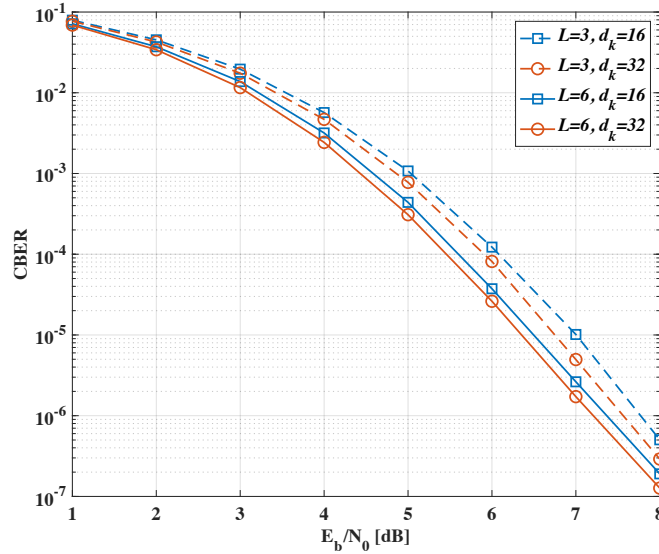
The results suggest that a deeper Transformer architecture is more capable of capturing intricate patterns and dependencies within the data, which is crucial for improving error correction performance. By adding more layers, the model can perform multiple levels of abstraction and refinement, allowing it to better understand and correct errors. This is especially crucial in the context of wireless communication systems, which are characterized by complexity and variability that simple models might not adequately capture.

In essence, the findings emphasize the importance of model depth in Transformer architectures for error correction tasks. This insight can guide the design of more effective models by prioritizing the depth of the encoder layers over the dimension of d_k , leading to better performance in practical applications.

5.2 Impact of the Sparse Masked Attention

We illustrate the impact of sparse masked attention on loss, CBER, and CBLER in Fig. 11. Specifically, sparse masked attention reduces the loss by 45% and leads to faster convergence during training. Furthermore, this approach significantly improves error correction performance: the CBER shows an improvement of approximately 0.4 dB at a bit error rate of 10^{-5} , and the CBLER improves by about 0.5 dB at a block error rate of 10^{-4} .

These improvements underscore the efficacy of integrating domain-specific knowledge into the attention mechanism, demonstrating substantial gains in both efficiency and accuracy. This approach not only reduces computational complexity but also enhances the model’s ability to decode complex signals, making it a promising strategy for future advancements in error correction techniques.


 Figure 9: BER for LDPC codes under $L = 6, d_k = 32$.

 Figure 10: CBER performance across various Transformer encoder layers and the dimensions d_k .

5.3 Computational Complexity Analysis

Before delving into the computational complexity, let's first review the unified error correction code Transformer presented in Figure 7, which incorporates L layers of Transformer encoders. The principal computational complexity within each layer is found in the multi-head self-attention module, which is predominantly responsible for matrix multiplication and is defined by the hyperparameters H, d_k and d_l . Consequently, the computational complexity of the proposed architecture is given by $O(L \times H \times (H_d \times d_k \times d_l \times N + d_k^2))$, where $N = 2n - k, d_l \ll N$ and $H \ll N$. Thanks to the sparsity of the parity-check matrix, H_d is usually quite small. In our experiment, H_d is approximately 0.17, which significantly reduces the computational complexity of the neural network.

In comparison, the approach in [22], which employs the vanilla Transformer architecture, has a complexity of $O(L \times H \times (N^2 \times d_k + d_k^2))$. When it comes to non-learning solutions, the computational complexities of the SCL and NMS decoding algorithms are $O(L_s \times n \times \log_2(n)) + O(L_s \times (n - 1)) + k \times O(2 \times L_s \times \log_2(2 \times L_s))$ and $I_{max} \times O(2 \times n \times d_v + M \times (2 \times d_c - 1)) + I_{max} \times O(M \times d_c)$, respectively [34]. Here, L_s is the list size, I_{max}

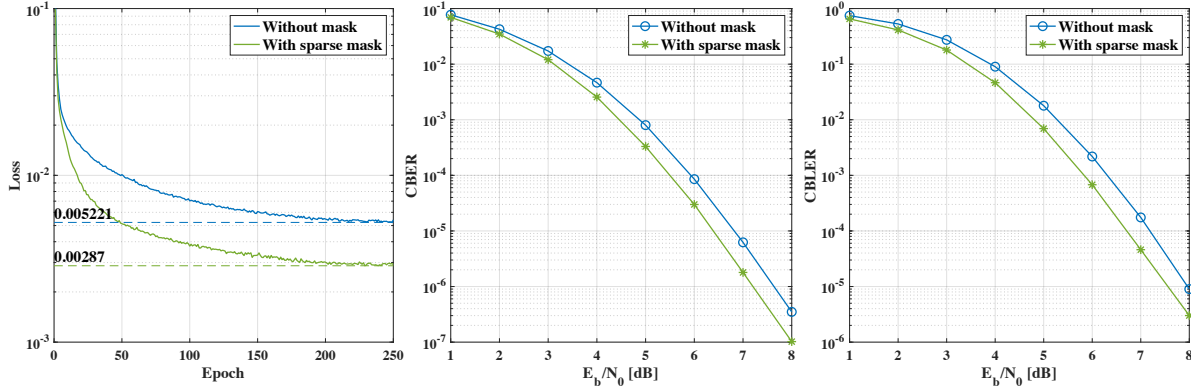


Figure 11: The overall improvement in loss, CBER and CBLER with sparse masked attention.

is the maximum number of iterations, M is the size of the check matrix, d_v is the number of variable node, and d_c is the number of parity check node.

Compared to the approach in [22], while the proposed method excels in decoding versatility and computational complexity, it may fall short in terms of memory efficiency, power consumption, and computational resource utilization when compared to non-learning solutions. This inefficiency could limit its potential for deployment. To address these issues, future implementations could leverage techniques such as parameter sharing, low-rank factorization, and quantization, aiming to reduce complexity and enhance efficiency [35, 36].

6 Conclusions

We introduced a novel, unified code-agnostic Transformer decoding architecture, designed to integrate various linear block codes seamlessly and offer superior decoding performance. Our approach leverages the self-attention mechanism inherent in Transformer models, enabling effective handling of sequential data and capturing long-range dependencies critical for decoding tasks. Through rigorous analysis and extensive experimental validation, our results indicate that the unified Transformer decoding architecture can significantly advance the state-of-the-art in decoding performance, potentially setting new benchmarks for future research and practical applications.

In conclusion, the unified Transformer decoding architecture presented in this paper signifies a significant step forward in the field of error correction coding. It paves the way for the development of more adaptable, efficient, and robust decoding solutions, poised to meet the stringent requirements of 6G and beyond. As the field progresses, we anticipate that the continued integration of AI technologies will unlock new possibilities, driving innovation in wireless communication systems. Future work can aim to further reduce hardware implementation complexity and enhance computational efficiency using techniques such as quantization and compression of neural network models.

References

- [1] Emil Björnson, Luca Sanguinetti, Henk Wymeersch, Jakob Hoydis, and Thomas L. Marzetta. Massive mimo is a reality – what is next? five promising research directions for antenna arrays. *Digit. Signal Process.*, 94:3–20, November 2019.
- [2] Marco Giordani, Michele Polese, Marco Mezzavilla, Sundeep Rangan, and Michele Zorzi. Toward 6G networks: use cases and technologies. *IEEE Commun. Mag.*, 58(3):55–61, March 2020.
- [3] Wei Jiang, Bin Han, Mohammad Asif Habibi, and Hans Dieter Schotten. The road towards 6G: a comprehensive survey. *IEEE open j. Commun. Soc.*, 2:334–366, 2021.
- [4] Erdal Arıkan. Channel polarization: a method for constructing capacity-achieving codes for symmetric binary-input memoryless channels. *IEEE Trans. Inf. Theory*, 55(7):3051–3073, July 2009.
- [5] R. Gallager. Low-density parity-check codes. *IEEE Trans. Inf. Theory*, 8(1):21–28, January 1962.
- [6] Huazi Zhang and Wen Tong. Channel coding for 6G extreme connectivity - requirements, capabilities and fundamental tradeoffs. *IEEE BITS Inf. Theory Mag.*, pages 1–12, 2024.

- [7] R.C. Bose and D.K. Ray-Chaudhuri. On a class of error correcting binary group codes. *Inf. Control*, 3(1):68–79, 1960.
- [8] Marvin Geiselhart, Felix Krieg, Jannis Clausius, Daniel Tandler, and Stephan Ten Brink. 6G: A welcome chance to unify channel coding? *IEEE BITS Inf. Theory Mag.*, 3(1):67–80, March 2023.
- [9] Camille Leroux, Ido Tal, Alexander Vardy, and Warren J. Gross. Hardware architectures for successive cancellation decoding of polar codes. In *2011 IEEE International Conference on Acoustics, Speech and Signal Processing (ICASSP)*, pages 1665–1668, Prague, Czech Republic, May 2011. IEEE.
- [10] M.P.C. Fossorier, M. Mihaljevic, and H. Imai. Reduced complexity iterative decoding of low-density parity check codes based on belief propagation. *IEEE Trans. Commun.*, 47(5):673–680, May 1999.
- [11] C. Spagnol, E.M. Popovici, and W.P. Marnane. Hardware implementation of $GF(2^m)$ LDPC decoders. *IEEE Trans. Circuits Syst. I, Reg. Pap.*, 56(12):2609–2620, December 2009.
- [12] Priya Mathew, Lismi Augustine, Sabarinath G., and Tomson Devis. Hardware implementation of (63,51) BCH encoder and decoder for WBAN using LFSR and BMA, August 2014. arXiv:1408.2908.
- [13] Shan Cao, Ting Lin, Shunqing Zhang, Shugong Xu, and Chuan Zhang. A reconfigurable and pipelined architecture for standard-compatible ldpc and polar decoding. *IEEE Trans. Veh. Technol.*, 70(6):5431–5444, June 2021.
- [14] Yufan Yue, Tutu Ajayi, Xueyang Liu, Peiwen Xing, Zihan Wang, David Blaauw, Ronald Dreslinski, and Hun Seok Kim. A unified forward error correction accelerator for multi-mode turbo, ldpc, and polar decoding. In *IEEE ISLPED*, pages 1–6, Boston MA USA, August 2022. ACM.
- [15] Ken R. Duffy, Jiange Li, and Muriel Medard. Capacity-achieving guessing random additive noise decoding. *IEEE Trans. Inf. Theory*, 65(7):4023–4040, July 2019.
- [16] Ken R. Duffy, Wei An, and Muriel Medard. Ordered reliability bits guessing random additive noise decoding. *IEEE Trans. Signal Process.*, 70:4528–4542, 2022.
- [17] Syed Mohsin Abbas, Thibaud Tonnellier, Furkan Ercan, Marwan Jalaeddine, and Warren J. Gross. High-throughput and energy-efficient VLSI architecture for ordered reliability bits GRAND. *IEEE Trans. Very Large Scale Integr. (VLSI) Syst.*, 30(6):681–693, June 2022.
- [18] E. Nachmani, E. Marciano, L. Lugosch, W. J. Gross, D. Burshtein, and Y. Be’ery. Deep learning methods for improved decoding of linear codes. *IEEE J. Sel. Topics Signal Process.*, 12(1):119–131, February 2018.
- [19] Jincheng Dai, Kailin Tan, Zhongwei Si, Kai Niu, Mingzhe Chen, H. Vincent Poor, and Shuguang Cui. Learning to decode protograph ldpc codes. *IEEE J. Sel. Areas Commun.*, 39(7):1983–1999, July 2021.
- [20] T. Gruber, S. Cammerer, J. Hoydis, and S. t. Brink. On deep learning-based channel decoding. In *2017 51st CISS*, pages 1–6, March 2017.
- [21] Ashish Vaswani, Noam Shazeer, Niki Parmar, Jakob Uszkoreit, Llion Jones, Aidan N Gomez, and Illia Polosukhin. Attention is all you need. In I. Guyon, U. Von Luxburg, S. Bengio, H. Wallach, R. Fergus, S. Vishwanathan, and R. Garnett, editors, *Advances in Neural Information Processing Systems*, volume 30. Curran Associates, Inc., 2017.
- [22] Yoni Choukroun and Lior Wolf. Error correction code transformer. In S. Koyejo, S. Mohamed, A. Agarwal, D. Belgrave, K. Cho, and A. Oh, editors, *Advances in Neural Information Processing Systems*, volume 35, pages 38695–38705. Curran Associates, Inc., 2022.
- [23] Kaiming He, Xiangyu Zhang, Shaoqing Ren, and Jian Sun. Deep residual learning for image recognition. In *IEEE CVPR*, June 2016.
- [24] Jimmy Lei Ba, Jamie Ryan Kiros, and Geoffrey E. Hinton. Layer normalization, 2016. arXiv:1607.06450.
- [25] A. Bennatan, Y. Choukroun, and P. Kisilev. Deep learning for decoding of linear codes - a syndrome-based approach. In *2018 IEEE ISIT*, pages 1595–1599, June 2018.
- [26] T.J. Richardson and R.L. Urbanke. The capacity of low-density parity-check codes under message-passing decoding. *IEEE Trans. Inf. Theory*, 47(2):599–618, February 2001.
- [27] Haoyi Zhou, Shanghang Zhang, Jieqi Peng, Shuai Zhang, Jianxin Li, Hui Xiong, and Wancai Zhang. Informer: beyond efficient transformer for long sequence time-series forecasting. *AAAI Conf. Artif. Intell. Proc.*, 35(12):11106–11115, May 2021.
- [28] E. Arikan. Systematic polar coding. *IEEE Commun. Lett.*, 15(8):860–862, August 2011.

- [29] Ruibin Xiong, Yunchang Yang, Di He, Kai Zheng, Shuxin Zheng, Chen Xing, Huishuai Zhang, Yanyan Lan, Liwei Wang, and Tieyan Liu. On layer normalization in the transformer architecture. In Hal Daumé III and Aarti Singh, editors, *37th ICML*, volume 119 of *Proceedings of machine learning research*, pages 10524–10533. PMLR, July 2020.
- [30] Diederik P. Kingma and Jimmy Ba. Adam: a method for stochastic optimization, January 2017. arXiv:1412.6980.
- [31] Michael Helmling, Stefan Scholl, Florian Gensheimer, Tobias Dietz, Kira Kraft, Stefan Ruzika, and Norbert Wehn. Database of channel codes and ML simulation results, 2019. Published: www.uni-kl.de/channel-codes.
- [32] Ido Tal and Alexander Vardy. List decoding of polar codes. *IEEE Trans. Inf. Theory*, 61(5):2213–2226, May 2015.
- [33] Jinghu Chen and M.P.C. Fossorier. Near optimum universal belief propagation based decoding of low-density parity check codes. *IEEE Trans. Commun.*, 50(3):406–414, March 2002.
- [34] Huawei. On latency and complexity. Technical Report R1-164040, 3rd Generation Partnership Project (3GPP), May 2016.
- [35] Beidi Chen, Tri Dao, Eric Winsor, Zhao Song, Atri Rudra, and Christopher Ré. Scatterbrain: unifying sparse and low-rank attention. In M. Ranzato, A. Beygelzimer, Y. Dauphin, P.S. Liang, and J. Wortman Vaughan, editors, *Adv. Neural Inf. Process. Syst.*, volume 34, pages 17413–17426. Curran Associates, Inc., 2021.
- [36] Zhenhua Liu, Yunhe Wang, Kai Han, Wei Zhang, Siwei Ma, and Wen Gao. Post-training quantization for vision transformer. *Adv. Neural Inf. Process. Syst.*, 34:28092–28103, 2021.